ACS Photonics

Article

pubs.acs.org/journal/apchd5

Multipolar Third-Harmonic Generation in Fishnet Metamaterials

Lei Wang,[†] Alexander S. Shorokhov,[‡] Pavel N. Melentiev,[§] Sergey Kruk,[†] Manuel Decker,[†] Christian Helgert,[†,⊥] Frank Setzpfandt,[†,⊥] Andrey A. Fedyanin,[‡] Yuri S. Kivshar,[†] and Dragomir N. Neshev*[,†]

[†]Nonlinear Physics Centre and CUDOS, Research School of Physics and Engineering, The Australian National University, ACT 2601, Canberra, Australia

[‡]Faculty of Physics, Lomonosov Moscow State University, Moscow 119991, Russia

[§]Institute for Spectroscopy, Moscow 142190, Russia

[⊥]Institute of Applied Physics, Abbe Center of Photonics, Friedrich-Schiller-Universität Jena, 07743 Jena, Germany

S *Supporting Information*

ABSTRACT: We study the third-harmonic generation from metal−dielectric−metal layered fishnet metamaterials and identify experimentally the multipolar contributions to the generated nonlinear harmonic fields by analyzing the radiation patterns of the emission. We observe that the third harmonic radiated from the fishnet structure is a result of the interference of the electric and magnetic dipoles and the electric quadrupole modes. Our results provide direct evidence of the importance of higher order multipoles in the nonlinear response of fishnet metamaterials, opening new opportunities for enhanced nonlinearities and controlled directionality of nonlinear processes in metamaterials.

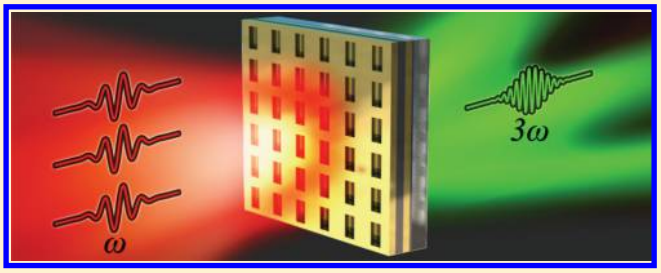

KEYWORDS: *nonlinear metamaterials, optical magnetism, third-harmonic generation, multipolar decomposition*

Nonlinear metamaterials and metasurfaces have recently attracted great attention[1,2] due to new possibilities for engineering their nonlinear optical response[3] and hence attaining enhanced actions based on magnetic-type nonlinearities.[4] In particular the interference between the electric and magnetic nonlinear contributions can lead to unidirectional harmonic generation even from an ultrathin metasurface.[5] Enabling such unidirectional emission would open a new range of applications, such as nonlinear mirrors for lasers, nonlinear luminescent markers for sensing, and nonlinear holography.

To explore these unique opportunities in metamaterials, a number of works have studied the possibilities to quantify the electric and magnetic contributions in optical harmonic generation and hence to control the directionality of the nonlinear emission. Optical second-harmonic generation (SHG) has been studied in split-ring resonator metasurfaces,[6,7] where the magnetic contribution of the SHG was derived from an equivalent circuit model. Further, nonlinear spectroscopy of fishnet metamaterials has been performed,[8] indicating the electric dipole nature of the harmonic emission. Most recently, the nonlinear properties of metamaterials have been studied in the context of Miller's rule, aiming to obtain the nonlinear susceptibilities of metamaterials from their linear properties.[9] However, since Miller's rule is derived solely from the electric-dipole nonlinear oscillator model, this rule cannot be directly applied to metamaterials, where the magnetic polarizability can be significant. Clearly, the higher order multipolar contributions in the nonlinear response need to be carefully accounted for.

While more accurate models taking into account the multipolar contribution of the nonlinear response have been explored theoretically,[10,11] the experimental techniques for such nonlinear multipolar analyses remain underdeveloped. This is an enduring problem, and a number of indirect techniques have been tested. It was possible to derive the multipolar contribution of the SHG process in plasmonic metasurfaces through the analysis of the nonlinear interference in forward/backward directions and for different incident polarizations.[12−15] Other indirect techniques also include noncollinear SHG[16] and multipolar decomposition through analyses of the broad spectrum nonlinear response of magnetic plasmonic metasurfaces.[17] However, the direct measurement of the different multipolar contributions from metamaterials with defined magnetic response has not been demonstrated to date.

Here, we demonstrate the direct experimental analysis of the multipolar origin of the third-harmonic generation (THG) from metamaterials with magnetic response. In particular, we measure, by a Fourier imaging technique, the radiation pattern of the THG from an optical metal−dielectric−metal fishnet metamaterial in the spectral vicinity of its optically induced magnetic resonance. Fitting the measured radiation pattern to the radiation patterns of different multipolar contributions from

Special Issue: Nonlinear and Ultrafast Nanophotonics

Received: January 18, 2016

DOI: 10.1021/acsphotonics.6b00040
ACS Photonics XXXX, XXX, XXX−XXX

the constituents of the metasurface shows that the observed third-harmonic radiation of the fishnet sample is a result of the interference between the magnetic and electric multipolar contributions of the nonlinear material polarization. Our results give direct evidence of the higher order multipolar contribution to the harmonic generation from magnetic metamaterials.

EXPERIMENTAL ARRANGEMENTS

The analysis of the linear radiation pattern from optical nanoantennas has been recently used as an experimental tool to identify the superposition of the involved electric and magnetic multipolar contributions.[18−20] Such analysis should also be applicable for the case of the nonlinear (second and third harmonic) emission;[21−25] however the experimental characterization of the nonlinear multipolar radiation from nanoantennas is still lacking. A Fourier analysis of the second-harmonic radiation from multipolar nanoantennas was recently performed in refs 26 and 27; however the multipolar contributions of this emission were not established. Here we perform such analysis, for the first time, to identify the multipolar origin of the harmonic generation process in metamaterials with magnetic response.

In our studies we use a metal−dielectric−metal fishnet structure in the spectral vicinity of the optically induced magnetic resonance (Figure 1). The fishnet metamaterials are exemplary metamaterial structures with a well-studied linear magnetic response[28,29] obtained due to the excitation of antiparallel currents in the top and bottom metal layers. The nonlinear response of the fishnets has also been experimentally studied for optical switching with fast[30] or slow nonlinearities,[31] as well as for SHG and THG.[8,32] Reference 32 has been focused on the exploration of harmonic contributions different from the electric dipole through angular-dependent THG measurements. However, only indirect evidence of nondipolar nonlinear terms was provided. A direct quantification of the higher order multipolar terms in the THG process is still missing.

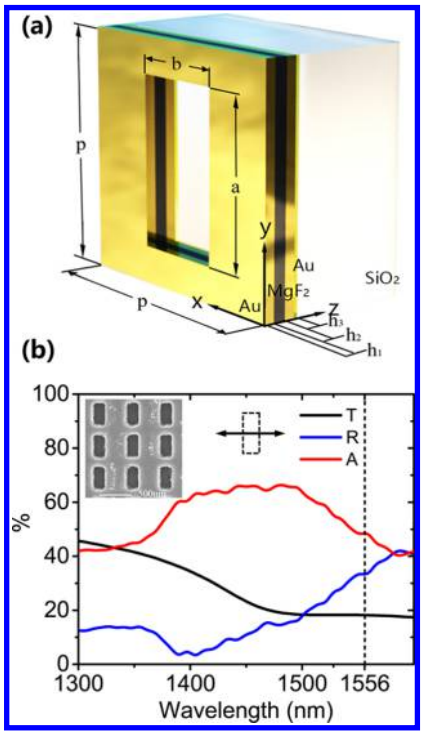

Figure 1. (a) Geometry of our fishnet metamaterial. The sizes are p = 500 nm; a = 350 nm; b = 190 nm; $h_1 = h_3$ = 20 nm; and h_2 = 25 nm. (b) Measured transmission (black curve), reflection (blue curve), and absorption (red curve) spectra of the fishnet for horizontal polarization of the incident light (i.e., electric field is parallel to the short side of the rectangular holes). The inset shows a scanning electron micrograph image of the fabricated sample. The vertical dashed line indicates the spectral position of the fundamental wavelength of the laser used in the THG setup.

To provide a quantitative experimental analysis of the harmonic generation process in magnetic metamaterials, we fabricate a sample of a fishnet metamaterial using electron beam lithography. The metamaterial consists of a trilayer Au/MgF_2/Au structure perforated periodically with holes. Figure 1a shows the dimensions of the unit cell; and the inset in Figure 1b shows a scanning electron micrograph of the structure. We measure the transmission and reflection spectra of the fishnet structure in order to determine its resonant absorption and hence to identify the position of the magnetic resonance (see Figure 1b). Measurements have been performed for both principal linear polarizations. The magnetic properties of the fishnet metamaterials are present only for horizontal polarization[33] (as marked in Figure 1b), while for vertical polarization the structure is not resonant and has low transmission. The resonance in the absorption spectrum was found to be around 1450 nm and is associated with a magnetic resonance in the structure. In our experiments we optically pump the fishnet metamaterial at a fundamental wavelength of 1556 nm, which is on the long-wavelength side of the maximal absorption wavelength, however within the resonance width.

We also experimentally determine the effective refractive index as well as the electric and magnetic surface polarizabilities of the metamaterial for linear horizontal polarization. For this purpose we measure the amplitude and phase of both transmission and reflection using interferometry methods similar to ref 34 (see Figure S1 in the Supporting Information). The phase measurements are performed in the spectral range 1530−1605 nm, which is defined by the spectral range of our CW laser light source, used for the interferometry. We then use inverted Fresnel equations to extract the effective refractive index[35] and surface polarizabilities[36] of the structure (see details in the Supporting Information). In particular, we find that at the pump wavelength of 1556 nm, the structure exhibits negative magnetic polarizability and a negative refractive index of $n = -0.62$.

We next numerically calculate the linear response of the fishnet structure in the spectral range of 1300−1600 nm using Lumerical FDTD solutions (see Figure S2 of the Supporting Information). Figure 2 depicts the calculated electric field magnitude inside the fishnet metamaterial at the fundamental wavelength of 1556 nm, showing 23-fold enhancement of the local field inside the middle dielectric layer (in comparison to the incident field). Figure 2a illustrates the electric field magnitude in the xy cross section, placed in the middle of the MgF_2 layer. The dashed white line shows the location of the rectangular hole. The xz cross section of the electric field magnitude is shown in Figure 2b. The cross section is taken through the center of the hole. The field distribution indicates that a standing wave is formed in the center of the dielectric layer by two plasmon currents, propagating in opposite directions at the interfaces between top and bottom gold layers and the dielectric slab (visualized by the vectorial E-field distribution in Figure 2b). These plasmon currents in the Au

DOI: 10.1021/acsphotonics.6b00040
ACS Photonics XXXX, XXX, XXX−XXX

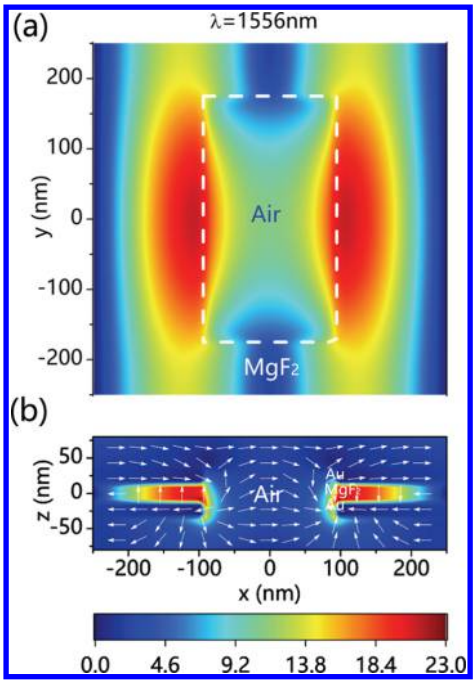

Figure 2. Calculated electric field magnitude (normalized to the incident field amplitude) inside the fishnet sample at the pump wavelength. (a) *xy* cross section of the field taken through the center of the MgF_2 layer. The dashed line shows the location of the rectangular hole. (b) *xz* cross section taken through the center of the hole.

layers together with the displacement currents running through the MgF_2 spacer layer form an effective optical magnetic response under the incident pump excitation. This is confirmed by the extraction of the effective index of the fishnet structure,[35] which becomes negative at the position of the absorption resonance, including the position of the fundamental wave (see Figure S3 of the Supporting Information). We use numerical results to calculate the effective refractive index of the structure and find that it matches well with the experimental values as seen in Figure S3 of the Supporting Information.

Next, we investigate the THG in our fishnet metamaterial. The THG nonlinear process is independent of the symmetry (centrosymmetric or anisotropic) of the constituent materials of the structure, which makes it attractive for the investigation of nonlinear optical phenomena in nanophotonics. The THG process is also extremely sensitive to the nanostructure resonances, which enhance the local electric field;[37−41] therefore we also expect enhanced nonlinear response from our fishnet metamaterials in the vicinity of its resonances. In our study we use the experimental setup depicted in Figure 3. A femtosecond Er^{3+}-doped fiber laser (~500 fs, repetition rate of 5 MHz) with a central wavelength of 1556 nm is used as a pump. The short femtosecond pulses allow achieving strong peak intensity and low average power at the same time, which prevents thermal damage of the sample. The pump laser beam passes through a combination of both quarter- and half-waveplates, which provides linear output polarization with controllable orientation.

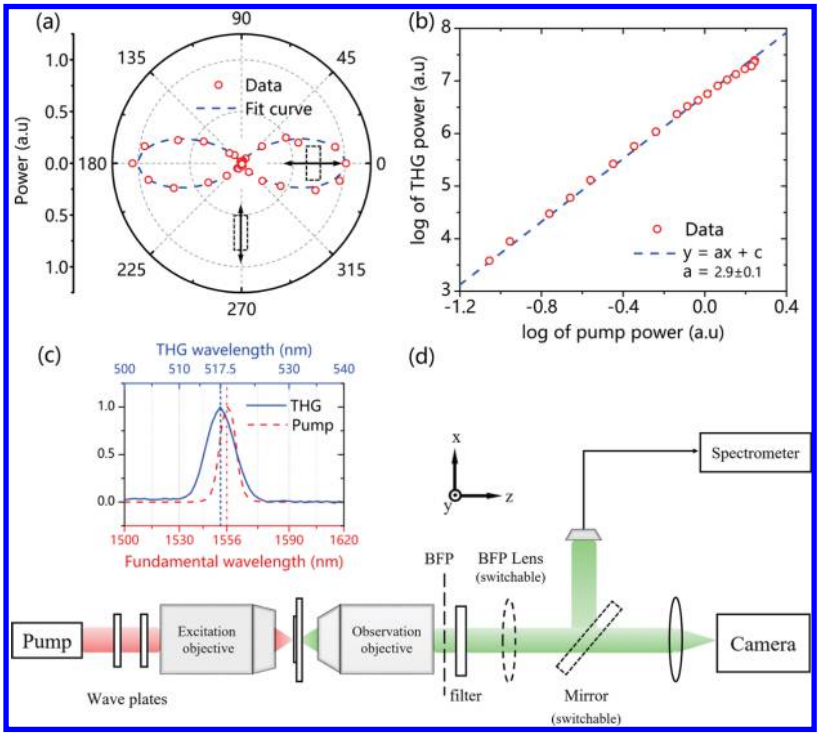

Figure 3. (a) Pump polarization dependency of the THG signal in polar coordinates. The zero angle corresponds to the case where the pump polarization is in the *x* direction. (b) Pump power dependency of the THG signal. The THG signal power as a function of the pump power, shown in a log scale, reveals a linear relation of $y = ax + c$, where $a = 2.9 \pm 0.1$, which matches the expected cubic relation between the pump and the THG signal power. (c) Measured THG and pump spectra (normalized to max value). The red curve represents the pump spectrum; the red *x*-axis is centered at the pump wavelength (1556 nm). The blue curve depicts the spectrum of the observed third harmonic on an axis corresponding to one-third of the fundamental wavelength. (d) Scheme of the experimental setup. The polarization of the pump beam is manipulated by a half-waveplate. The THG is generated and observed by a confocal microscopic setup. The bandpass filter at the THG wavelength is used for the radiation pattern imaging.

DOI: 10.1021/acsphotonics.6b00040
ACS Photonics XXXX, XXX, XXX−XXX

An infrared objective lens (Olympus LCPlanN 100×, NA = 0.85) is used to focus the pump laser beam onto the sample top gold surface to a diameter of ∼2 μm, exciting approximately 12 unit cells of the structure (see details in the Supporting Information). The output emission pattern is then a result of the superposition of radiation from several localized third-harmonic emitters, positioned in a periodic array. The THG signal is collected by a confocal visible objective (Olympus MPlanFL 50×, NA = 0.8). The metal surface of the sample is facing the pump laser. Then the third-harmonic radiation is either launched into a spectrometer (Ocean Optics 6500) or sent to a Peltier-cooled camera with an infinity-corrected objective to build a real-space image. For the imaging purposes, a 520 nm (±10 nm) bandpass filter is used to transmit the third-harmonic radiation only, thus preventing unwanted transmission of the fundamental wavelength from being captured by the camera. A switchable mirror is used to change the beam path between the spectrometer and the camera.

Figure 3a shows the dependency of the third-harmonic intensity versus the direction of polarization of the pump. In the polar coordinate system the zero angle corresponds to the horizontally polarized pump, as indicated in the figure. The radial coordinate represents the third-harmonic power, measured by the spectrometer. Figure 3b shows the power dependency of the THG. The pump power is adjusted with a continuously variable neutral density filter and is monitored by a power meter. The THG power (in a logarithmic scale) obeys an approximately linear relation that gives us $P_{THG} = CP_{pump}^{2.9 \pm 0.1}$, which matches well the expected cubic relation between the pump and the THG power. Figure 3c shows the spectra of the pump (red dashed curve, bottom axis) and THG (blue curve, top axis). The overlap between the THG and the pump spectra confirms that the measured signal is indeed a third harmonic and not photoluminescence from the sample. Note that the presence of the plasmonic resonances at the fundamental frequency can substantially change the spectrum of the THG emission.[42] The measured small blue spectral shift of THG emission (∼1.2 nm) is a consequence of the fact that the magnetic resonance of the fishnet is blue-shifted in comparison to the fundamental wavelength.

RESULTS AND ANALYSIS

To analyze the nonlinear properties of the fishnet sample, we measure the directionality of the third-harmonic radiation. A switchable Bertrand (back focal plane, BFP) lens is used to capture the Fourier space image of the third-harmonic radiation (i.e., the angular distribution of the radiation pattern), as illustrated in Figure 3d. In this way we can build a BFP image of the THG on our camera. We observe three distinct maxima located along the x direction, as seen in Figure 4a. The circular boundary around the figure represents the numerical aperture of our system, which equals 0.8. That corresponds to a 33° maximal propagation angle inside the substrate.

In order to gain a deeper insight into the origin of the THG radiation pattern, we use the multipole model to analyze its spatial structure. For this we start with expansion of the vector potential in the far zone ($kr \gg 1$) in powers of k considering the dimension of the source to be small compared to the wavelength ($kd \ll 1$):

$$\lim_{kr\to\infty} \mathbf{A}(\mathbf{x}) = \frac{\mu_0}{4\pi}\frac{e^{ikr}}{r}\sum_n \frac{(-ik)^n}{n!}\int \mathbf{J}(\mathbf{x}')(\mathbf{n}\cdot\mathbf{x}')^n d^3x' \quad (1)$$

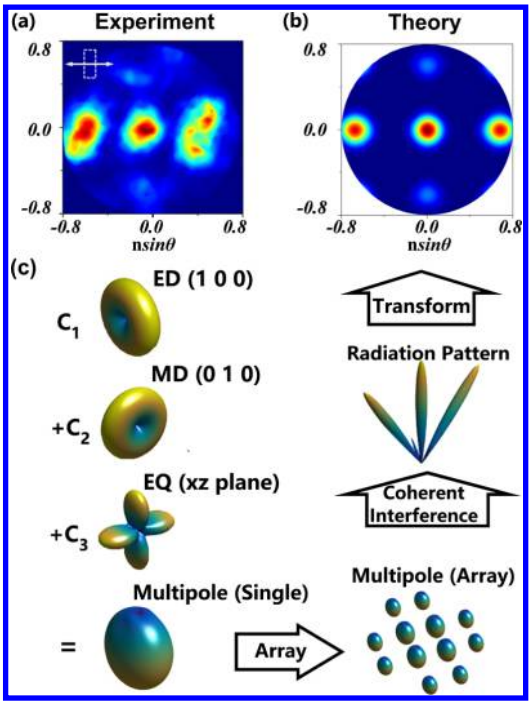

Figure 4. (a) Measured directionality of the THG radiation. The numerical aperture of the captured THG signal is 0.8. (b) Calculated BFP image using the multipole model and optimized parameters. (c) Schematics of the multipole model. We select the first terms of the multipolar series including ED, MD, and EQ, each represented by the shapes of their radiation pattern. The spatial orientations of the multipoles are defined by the geometry of the metamaterial. The electromagnetic field of the metamaterial unit cell is the superposition of the ED, MD, and EQ fields with complex amplitudes C_1, C_2, and C_3. The resulting field is an interference of the emission from several unit cells illuminated with the focused pump beam.

where $\mathbf{x}$ is the vector from the origin (0, 0, 0) to a certain point (x_1, x_2, x_3) in the far zone, $\mathbf{n}$ is the unity vector in the direction of $\mathbf{x}$, r is the length of $\mathbf{x}$, $\mathbf{x}'$ is the vector from the origin to a certain source point, and $\mathbf{J}(\mathbf{x})'$ is the current density.[43]

The first term gives the electric dipole (ED) radiation:

$$\mathbf{H}_{ED} = \frac{ck^2}{4\pi}(\mathbf{n}\times\mathbf{p})\frac{e^{ikr}}{r} \quad (2)$$

where the ED moment $\mathbf{p} = \int \mathbf{x}'\rho(\mathbf{x}')d^3x'$, $\rho(\mathbf{x}')$ is the charge density distribution, and $Z_0 = \sqrt{\mu_0/\epsilon_0}$ is the free space impedance.

The next terms of the expansion give a magnetic dipole (MD) and an electric quadrupole (EQ) response. The MD term can be written as

$$\mathbf{H}_{MD} = \frac{k^2}{4\pi}(\mathbf{n}\times\mathbf{m})\times\mathbf{n}\frac{e^{ikr}}{r} \quad (3)$$

where $\mathbf{m} = \frac{1}{2}\int(\mathbf{x}'\times\mathbf{J}(\mathbf{x}'))d^3x'$ is the MD moment.

The EQ radiation is represented as

$$\mathbf{H}_{EQ} = -\frac{ick^3}{24\pi}(\mathbf{n}\times\mathbf{Q}(\mathbf{n}))\frac{e^{ikr}}{r} \quad (4)$$

The vector $\mathbf{Q}(\mathbf{n}) = (Q_1, Q_2, Q_3)$ is defined as $Q_\alpha = \sum_\beta Q_{\alpha\beta}n_\beta$, where $\alpha,\beta = 1, 2$, and 3. $Q_{\alpha\beta} = \int(3x'_\alpha x'_\beta - r'^2\delta_{\alpha\beta})\rho(\mathbf{x}')d^3x'$ is the quadrupole moment tensor.

DOI: 10.1021/acsphotonics.6b00040
ACS Photonics XXXX, XXX, XXX−XXX

The spatial orientations of the multipoles can be predefined by the simulated field results in Figure 2. The electrons in the metal layers are considered as oscillators along the *xz*-plane. Therefore, the symmetric parallel currents will create ED radiation, while the antiparallel currents lead to MD radiation. The antisymmetric charge distribution along the *xz*-plane gives rise to the EQ with only $Q_{xz} = Q_{xz} \neq 0$. The corresponding radiation patterns of the considered multiple terms are shown in Figure 4c.

The electromagnetic field of the THG could be considered as the coherent superposition of the fields emitted by various multipoles. Considering only the first three terms, the total field can be written as $\mathbf{H}_{\text{multi}} = C_1\mathbf{H}_{\text{ED}} + C_2\mathbf{H}_{\text{MD}} + C_3\mathbf{H}_{\text{EQ}}$, where C_α are complex coefficients. The electric field is $\mathbf{E}_{\text{multi}} = Z_0\mathbf{H}_{\text{multi}} \times \mathbf{n}$. In these equations the relative amplitudes and phase of the multipoles are fitting parameters. Then the radiation pattern could be calculated via the time-averaged Poynting vector given by $\langle \mathbf{S} \rangle = \frac{1}{2}\text{Re}(\mathbf{E}_{\text{multi}} \times \mathbf{H}^*_{\text{multi}})$. The radiation power distribution can be written as the power radiated per unit angle: $\frac{\text{dP}}{\text{d}\Omega} = \mathbf{n}\cdot\langle \mathbf{S} \rangle r^2$.

Due to the larger size of the focal spot of the pump laser (diameter of around 2 μm) in comparison to the period of the fishnet (0.5 μm) in our analysis, we also consider the nonlinear emission from an array of third-harmonic emitters: the central unit cell and the second nearest neighbors. The multipole model also takes this array effect into account by considering each unit cell as an individual multipolar emitter. Their phases and amplitudes are defined by the Gaussian beam profile of the pump with a corresponding waist size. We also take into account the effect of the substrate on the effective period of the emitter array. Then the resulting field takes the form

$$\mathbf{H}_{\text{array}}(\mathbf{x}) = \text{e}^{-s_n^2/w^2} \sum_{\mathbf{s}_n} \mathbf{H}_{\text{multi}}(\mathbf{x} - \mathbf{s}_n) \tag{5}$$

where s_n is the vector from the origin to the location of the nth element of the array and w is the beam waist size.

From our analysis we obtain that the THG emission is a coherent superposition of an electric dipole, a magnetic dipole, and an electric quadrupole mode. The amplitude ratios of the multipolar modes are $A_{\text{ED}}/A_{\text{EQ}} = 1.58$ and $A_{\text{MD}}/A_{\text{EQ}} = 1.33$. Since our experimental measurements provide us only with the intensities of THG, we could not uniquely identify the set of relative phases. Therefore, our multipolar analysis results in two sets of phase differences that give identical results (for the same amplitude ratios). One set is $\varphi_{\text{ED}} - \varphi_{\text{EQ}} = -0.25\pi$ and $\varphi_{\text{MD}} - \varphi_{\text{EQ}} = 0.92\pi$, while the other set is $\varphi_{\text{ED}} - \varphi_{\text{EQ}} = -0.75\pi$ and $\varphi_{\text{MD}} - \varphi_{\text{EQ}} = 0.08\pi$. The calculated Fourier space image of the multipolar radiation is shown in Figure 4b and agrees very well with the experimental measurements. These results also agree qualitatively with an earlier theoretical study on the complementary metal–dielectric–metal structures.[17]

CONCLUSIONS

In summary, we built on the strong efforts to identify the multipolar nature of the harmonic generation in metamaterials and nanostructures. In particular, following previous works on THG in fishnet structures[32] we have established a new technique for identification of the multipolar (magnetic dipole and electric quadrupole) contributions to the nonlinear optical response of magnetic metamaterials. By an effectively single-shot technique, we have quantified these contributions for the THG process in fishnet metamaterials. Our results show that the nonlinear emission is indeed a superposition of several multipoles with a strong contribution from the electric quadrupole and magnetic dipole modes.

Our method of optical diagnostics provides a fast and convenient way to acquire the information on materials' nonlinear responses and links the nonlinear behaviors of the materials to their intrinsic properties. This paves the way toward the designs of various functional ultracompact nonlinear optical devices, including devices for highly directional nonlinear emission based on the coherent superposition of higher order multipoles such as nonlinear holograms.

ASSOCIATED CONTENT

Supporting Information

The Supporting Information is available free of charge on the ACS Publications website at DOI: 10.1021/acsphotonics.6b00040.

Additional information (PDF)

AUTHOR INFORMATION

Corresponding Author

*E-mail: dragomir.neshev@anu.edu.au.

Notes

The authors declare no competing financial interest.

ACKNOWLEDGMENTS

We acknowledge the financial support of the Australian Research Council under the Discovery and Centre of Excellence programs, the Russian Science Foundation (Grants #14-12-01144 - FDTD calculations and modeling, and #14-12-00729 - optical setup creation), and the Russian Foundation for Basic Research. We acknowledge the support of the ANFF ACT Node in carrying out the sample fabrication in this work. C.H. acknowledges a postdoctoral fellowship from the German Academic Exchange Service (DAAD).

REFERENCES

(1) Lapine, M.; Shadrivov, I. V.; Kivshar, Y. S. *Colloquium*: Nonlinear metamaterials. *Rev. Mod. Phys.* **2014**, *86*, 1093–1123.

(2) Minovich, A. E.; Miroshnichenko, A. E.; Bykov, A. Y.; Murzina, T. V.; Neshev, D. N.; Kivshar, Y. S. Functional and nonlinear optical metasurfaces. *Laser & Photon. Rev.* **2015**, *9*, 195–213.

(3) Kauranen, M.; Zayats, A. V. Nonlinear plasmonics. *Nat. Photonics* **2012**, *6*, 737–748.

(4) Pendry, J.; Holden, A.; Robbins, D.; Stewart, W. Magnetism from conductors and enhanced nonlinear phenomena. *IEEE Trans. Microwave Theory Tech.* **1999**, *47*, 2075–2084.

(5) Rose, A.; Huang, D.; Smith, D. R. Nonlinear Interference and Unidirectional Wave Mixing in Metamaterials. *Phys. Rev. Lett.* **2013**, *110*, 063901.

(6) Klein, M. W.; Enkrich, C.; Wegener, M.; Linden, S. Second-Harmonic Generation from Magnetic Metamaterials. *Science* **2006**, *313*, 502–504.

(7) Klein, M. W.; Wegener, M.; Feth, N.; Linden, S. Experiments on second- and third-harmonic generation from magnetic metamaterials. *Opt. Express* **2007**, *15*, 5238–5247.

(8) Kim, E.; Wang, F.; Wu, W.; Yu, Z.; Shen, Y. Nonlinear optical spectroscopy of photonic metamaterials. *Phys. Rev. B: Condens. Matter Mater. Phys.* **2008**, *78*, 113102.

(9) O'Brien, K.; Suchowski, H.; Rho, J.; Salandrino, A.; Kante, B.; Yin, X.; Zhang, X. Predicting nonlinear properties of metamaterials from the linear response. *Nat. Mater.* **2015**, *14*, 379–383.

DOI: 10.1021/acsphotonics.6b00040
ACS Photonics XXXX, XXX, XXX–XXX

(10) Ciracì, C.; Poutrina, E.; Scalora, M.; Smith, D. R. Origin of second-harmonic generation enhancement in optical split-ring resonators. *Phys. Rev. B: Condens. Matter Mater. Phys.* **2012**, *85*, 201403.
(11) Poutrina, E.; Huang, D.; Urzhumov, Y.; Smith, D. R. Nonlinear oscillator metamaterial model: numerical and experimental verification. *Opt. Express* **2011**, *19*, 8312−8319.
(12) Kujala, S.; Canfield, B. K.; Kauranen, M.; Svirko, Y.; Turunen, J. Multipole Interference in the Second-Harmonic Optical Radiation from Gold Nanoparticles. *Phys. Rev. Lett.* **2007**, *98*, 167403.
(13) Bachelier, G.; Russier-Antoine, I.; Benichou, E.; Jonin, C.; Brevet, P.-F. Multipolar second-harmonic generation in noble metal nanoparticles. *J. Opt. Soc. Am. B* **2008**, *25*, 955−960.
(14) Zdanowicz, M.; Kujala, S.; Husu, H.; Kauranen, M. Effective medium multipolar tensor analysis of second-harmonic generation from metal nanoparticles. *New J. Phys.* **2011**, *13*, 023025.
(15) Huttunen, M. J.; Mäkitalo, J.; Bautista, G.; Kauranen, M. Multipolar second-harmonic emission with focused Gaussian beams. *New J. Phys.* **2012**, *14*, 113005.
(16) Bovino, F. A.; Larciprete, M. C.; Sibilia, C.; Váró, G.; Gergely, C. Evidence of multipolar response of Bacteriorhodopsin by noncollinear second harmonic generation. *Opt. Express* **2012**, *20*, 14621−14631.
(17) Kruk, S.; Weismann, M.; Bykov, A. Y.; Mamonov, E. A.; Kolmychek, I. A.; Murzina, T.; Panoiu, N. C.; Neshev, D. N.; Kivshar, Y. S. Enhanced Magnetic Second-Harmonic Generation from Resonant Metasurfaces. *ACS Photonics* **2015**, *2*, 1007−1012.
(18) Taminiau, T. H.; Karaveli, S.; van Hulst, N. F.; Zia, R. Quantifying the magnetic nature of light emission. *Nat. Commun.* **2012**, *3*, 979.
(19) Hancu, I. M.; Curto, A. G.; Castro-López, M.; Kuttge, M.; van Hulst, N. F. Multipolar Interference for Directed Light Emission. *Nano Lett.* **2014**, *14*, 166−171.
(20) Kruk, S. S.; Decker, M.; Staude, I.; Schlecht, S.; Greppmair, M.; Neshev, D. N.; Kivshar, Y. S. Spin-Polarized Photon Emission by Resonant Multipolar Nanoantennas. *ACS Photonics* **2014**, *1*, 1218−1223.
(21) Bennemann, K. *Non-linear Optics in Metals*; International Series of Monographs on Physics; Clarendon Press, 1998.
(22) Dadap, J. I.; Shan, J.; Eisenthal, K. B.; Heinz, T. F. Second-Harmonic Rayleigh Scattering from a Sphere of Centrosymmetric Material. *Phys. Rev. Lett.* **1999**, *83*, 4045−4048.
(23) Makeev, E.; Skipetrov, S. Second harmonic generation in suspensions of spherical particles. *Opt. Commun.* **2003**, *224*, 139−147.
(24) Mäkitalo, J.; Suuriniemi, S.; Kauranen, M. Enforcing symmetries in boundary element formulation of plasmonic and second-harmonic scattering problems. *J. Opt. Soc. Am. A* **2014**, *31*, 2821−2832.
(25) Smirnova, D. A.; Khanikaev, A. B.; Smirnov, L. A.; Kivshar, Y. S. Multipolar third-harmonic generation driven by optically-induced magnetic resonances. *ACS Photonics* **2016**, 1456313.
(26) Viarbitskaya, S.; Demichel, O.; Cluzel, B.; Colas des Francs, G.; Bouhelier, A. Delocalization of Nonlinear Optical Responses in Plasmonic Nanoantennas. *Phys. Rev. Lett.* **2015**, *115*, 197401.
(27) Wolf, D.; Schumacher, T.; Lippitz, M. Shaping the nonlinear near field. *Nat. Commun.* **2016**, *7*, 10361.
(28) Zhang, S.; Fan, W.; Panoiu, N. C.; Malloy, K. J.; Osgood, R. M.; Brueck, S. R. J. Experimental Demonstration of Near-Infrared Negative-Index Metamaterials. *Phys. Rev. Lett.* **2005**, *95*, 137404.
(29) Dolling, G.; Enkrich, C.; Wegener, M.; Soukoulis, C. M.; Linden, S. Simultaneous Negative Phase and Group Velocity of Light in a Metamaterial. *Science* **2006**, *312*, 892−894.
(30) Dani, K. M.; Ku, Z.; Upadhya, P. C.; Prasankumar, R. P.; Brueck, S. R. J.; Taylor, A. J. Subpicosecond Optical Switching with a Negative Index Metamaterial. *Nano Lett.* **2009**, *9*, 3565−3569.
(31) Minovich, A.; Farnell, J.; Neshev, D. N.; McKerracher, I.; Karouta, F.; Tian, J.; Powell, D. A.; Shadrivov, I. V.; Hoe Tan, H.; Jagadish, C.; Kivshar, Y. S. Liquid crystal based nonlinear fishnet metamaterials. *Appl. Phys. Lett.* **2012**, *100*, 121113.
(32) Reinhold, J.; Shcherbakov, M. R.; Chipouline, A.; Panov, V. I.; Helgert, C.; Paul, T.; Rockstuhl, C.; Lederer, F.; Kley, E.-B.; Tünnermann, A.; Fedyanin, A. A.; Pertsch, T. Contribution of the magnetic resonance to the third harmonic generation from a fishnet metamaterial. *Phys. Rev. B: Condens. Matter Mater. Phys.* **2012**, *86*, 115401.
(33) Minovich, A.; Neshev, D. N.; Powell, D. A.; Shadrivov, I. V.; Lapine, M.; McKerracher, I.; Hattori, H. T.; Tan, H. H.; Jagadish, C.; Kivshar, Y. S. Tilted response of fishnet metamaterials at near-infrared optical wavelengths. *Phys. Rev. B: Condens. Matter Mater. Phys.* **2010**, *81*, 115109.
(34) Kruk, S. S.; Wong, Z. J.; Pshenay-Severin, E.; O'Brien, K.; Neshev, D. N.; Kivshar, Y. S.; Zhang, X. Magnetic hyperbolic optical metamaterials. *Nat. Commun.* **2016**, *7*, 11329.
(35) Smith, D. R.; Schultz, S.; Markoš, P.; Soukoulis, C. M. Determination of effective permittivity and permeability of metamaterials from reflection and transmission coefficients. *Phys. Rev. B: Condens. Matter Mater. Phys.* **2002**, *65*, 195104.
(36) Albooyeh, M.; Kruk, S.; Menzel, C.; Helgert, C.; Kroll, M.; Krysinski, A.; Decker, M.; Neshev, D. N.; Pertsch, T.; Etrich, C.; Rockstuhl, C.; Tretyakov, S. A.; Simovski, C. R.; Kivshar, Y. S. Resonant metasurfaces at oblique incidence: interplay of order and disorder. *Sci. Rep.* **2014**, *4*, 4484.
(37) Lippitz, M.; van Dijk, M. A.; Orrit, M. Third-Harmonic Generation from Single Gold Nanoparticles. *Nano Lett.* **2005**, *5*, 799−802.
(38) Aouani, H.; Rahmani, M.; Navarro-Cia, M.; Maier, S. A. Third-harmonic-upconversion enhancement from a single semiconductor nanoparticle coupled to a plasmonic antenna. *Nat. Nanotechnol.* **2014**, *9*, 290−294.
(39) Metzger, B.; Schumacher, T.; Hentschel, M.; Lippitz, M.; Giessen, H. Third Harmonic Mechanism in Complex Plasmonic Fano Structures. *ACS Photonics* **2014**, *1*, 471−476.
(40) Li, G.; Chen, S.; Pholchai, N.; Reineke, B.; Wong, P. W. H.; Pun, E. Y. B.; Cheah, K. W.; Zentgraf, T.; Zhang, S. Continuous control of the nonlinearity phase for harmonic generations. *Nat. Mater.* **2015**, *14*, 607−612.
(41) Shcherbakov, M. R.; Neshev, D. N.; Hopkins, B.; Shorokhov, A. S.; Staude, I.; Melik-Gaykazyan, E. V.; Decker, M.; Ezhov, A. A.; Miroshnichenko, A. E.; Brener, I.; Fedyanin, A. A.; Kivshar, Y. S. Enhanced Third-Harmonic Generation in Silicon Nanoparticles Driven by Magnetic Response. *Nano Lett.* **2014**, *14*, 6488−6492.
(42) Melentiev, P. N.; Afanasiev, A. E.; Kuzin, A. A.; Gusev, V. M.; Kompanets, O. N.; Esenaliev, R. O.; Balykin, V. I. Split Hole Resonator: A Nanoscale UV Light Source. *Nano Lett.* **2016**, *16*, 1138−1142.
(43) Jackson, J. *Classical Electrodynamics*; Wiley, 1998.

DOI: 10.1021/acsphotonics.6b00040
ACS Photonics XXXX, XXX, XXX−XXX